SUPPORTING INFORMATION FOR:

GPR55 controls functional differentiation of self-renewing epithelial progenitors for salivation

Solomiia Korchynska, Mirjam I. Lutz, Erzsébet Borók, Johannes Pammer, Valentina Cinquina, Nataliya Fedirko, Andrew J. Irving, Ken Mackie, Tibor Harkany and Erik Keimpema

Supporting Text on GPCR signaling

Since 2-arachidonoylglycerol (1) and arachidonoyl ethanolamine (2), endogenous ligands of type 1 and 2 cannabinoid receptors (CB_1Rs/CB_2Rs) (3, 4), purportedly bind GPR55 (5) and have been implicated in the control of salivation (6, 7), we also tested if CB_1Rs are co-expressed with GPR55 in ductal cells. At the mRNA level, we find CB_1R transcripts by qPCR in total submandibular gland extracts (Fig. 1D). Immunohistochemistry revealed CB_1Rs exclusively on parasympathetic nerves (Supporting Fig. 2D,E). Even though we find CB_2R transcripts in bulk mRNA of salivary glands, in situ hybridization remains inconclusive to assign CB_2Rs to specific cell types (Human Protein Atlas), which can include circulating myeloid lineages with high CB_2R content (8).

A shared theme among lipid receptor signaling pathways is continued receptor expression from progenitor to differentiated cell states acting as checkpoints for cell division and regulating exocytosis, respectively. For instance, CB_1Rs promote neurogenesis (9, 10) but later limit neurotransmitter release (11) in adult-born neurons of the hippocampus. Conversely, loss of CB_1Rs lowers proliferation and production of mature hepatocytes in zebrafish livers, impairing liver metabolism (12). In the immune system, CB_2Rs play a crucial role in the proliferation (13), migration (14) and cytokine production of immune cells (15). Likewise, the non-cannabinoid lipid sphingosine-1-phosphate negatively couples to T-cell proliferation (16) and differentiation (17), as well as interleukin synthesis (18). In the endocrine pancreas, GPR40, GPR119 and GPR120 all increase proliferation of beta-cells (19, 20), while also modulating insulin secretion (21–23). Our finding that GPR55 can control both proliferation and function in a stem cell-to-granular duct cell axis follows general rules observed for many G protein coupled lipid receptor systems. Thus, by conceptually incorporation GPR55 in a broad GPCR framework, we propose

the existence of a general rule along an axis from stem cell-to-differentiated progeny which in salivary glands identifies a GPR55 sensitive epithelial-granular duct niche.

Supporting Materials and Methods

In situ hybridization

Mouse submandibular glands were frozen in liquid N_2 and sectioned directly onto electrically-charged glass coverslips (14-µm thickness; SuperFrost$^+$). Sections were washed once in PBS and subsequently fixed with 4% PFA for 10 minutes. After hybridization, tissues were incubated with alkaline phosphatase-conjugated anti-digoxigenin antibody (Sigma), developed with NBT/BCIP (Roche) and mounted with Fluorescence Mounting Medium (Dako). For human tissues, paraffin-embedded sections were deparaffinized, and digested with proteinase K (20 µg/ml). After hybridization, they incubated with alkaline phosphatase-conjugated anti-digoxigenin antibody and developed with NBT/BCIP. Sections were counterstained with Mayer's hemalum solution and coverslipped with Fluorescence Mounting Medium (DAKO).

Antibody validation

Until now, the (sub)-cellular localization of GPR55 has been hotly debated due to the lack of reliable antibodies against GPR55. Therefore, we have extensively tested batches of our custom-made rabbit anti-GPR55 antibodies (Mouse GPR55 epitope: KEFRMRIKAHRPSTIKLVNQDTMVSRG) to verify their specificity. First, we have simultaneously processed wild-type and *Gpr55*$^{-/-}$ mouse salivary glands for dilution tests (1:3 dilution steps, up to 1:16,000), revealing clearly patterned residual staining in tight cell clusters resembling striated ducts, but not in granulated ducts (Fig. 2) in wild-type mice, confirming its relevance for these structures. Staining of *Gpr55*$^{-/-}$ tissues were negative at the concentration range used throughout. GPR55 showed graded abundance in submandibular > parotid = sublingual glands, with sublingual glands containing residual nuclear but not membranous staining in *Gpr55*$^{-/-}$ glands (Fig. 2). Therefore, and to avoid any controversy, we have exclusively focused on functional determination of GPR55 in the submandibular and parotid glands. The human submandibular and parotid glands exhibited GRP55 distribution patterns indistinguishable from those in mice. Omission of primary antibody on human tissues led to the complete absence of immunoreactivity (Fig. 2A). Second, we have verified the existence of *Gpr55* mRNA in both mouse and human salivary gland by in situ hybridization. Notably, we have found overlapping patterns between mRNA and protein localization, supporting our histochemical data (Fig. 1). Third, we have tested our GPR55 antibody on a HEK293 overexpression system. We transfected HEK293 cells (ATCC) with HA-tagged human GPR55 using Lipofectamine 2000, and found

co-localization only in transfected cells (Fig. 2C). Finally, we have tested our antibodies on mouse brains since recent results suggest GPR55-positive cellular structures in mouse hippocampus (24, 25). However, we were unable to detect credible DAB signal in healthy adult mouse hippocampus, striatum and cortex (Fig. 2B), which corroborates negative and/or very low GPR55 levels in in situ hybridization data of the adult mouse (Allen Brain Atlas; mouse.brain-map.org/experiment/show/79591399) (26).

Immunohistochemistry

Human salivary gland sections were deparaffinized and rehydrated, then treated with 3% H_2O_2 in methanol to block endogenous peroxidases and incubated with 10 mM citrate buffer (pH 6.0) at 95 ˚C for antigen retrieval. Sections were blocked with 10% fetal bovine serum and stained overnight with antibodies as listed (Supporting Table 3). DAKO's EnVision detection kit was used to amplify reaction products upon horseradish peroxidase-driven conversion of 3,3'-diaminobenzidine (DAB) with H_2O_2 used as substrate (0.01% in 0.05M Tris-HCl, pH 8.0; DAKO). Sections were counterstained with Mayer's hemalum solution (Merck), dehydrated in an ascending concentration gradient of ethanol, cleared with xylene and coverslipped with Consil-Mount (Thermo Scientific).

Sections from mouse submandibular glands were blocked with 5% normal donkey serum (NDS; Jackson), 2% bovine serum albumin (BSA; Sigma) and 0.3% Triton X-100 (Sigma) in 0.01M PBS. Tissues were incubated with a cocktail of antibodies (Supporting Table 3) in 2% NDS, 0.1% BSA and 0.3% Triton X-100 in PBS at 4˚C overnight. Secondary antibodies (1:300; Jackson ImmunoResearch) were applied in 2% BSA/PBS at 22-24 ºC for 2h. Sections were then treated with Autofluorescence Eliminator (Millipore) to quench autofluorescence and counterstained with Hoechst 33,342 (Sigma) to visualize nuclei before being coverslipped with Fluoromount (Sigma). We used *Solanum tuberosum* lectin (STL, Vector Labs, 2 µg/ml final concentration) for the fluorescent detection of glycoproteins (27). STL strongly labelled glycoprotein-containing vesicles in granulated ducts *vs.* weakly-contoured cell membranes in serous acinar, thus differentiating these structures (Fig. 1).

Immunocytochemistry

Fixed salispheres on coverslips (4% PFA) were blocked and permeabilized with 10% NDS, 5% BSA and 0.3% Triton X-100 in 0.01M PBS (pH7.4), and subsequently incubated with primary antibodies (Supporting Information, Supporting Table 3) in 2% NDS, 0.1% BSA and 0.3% Triton X-100 at 4 ˚C overnight. Alexa 488/555/647-conjugated secondary antibodies (1:300; Jackson ImmunoResearch) were diluted in 2% BSA in 0.01M PBS (pH 7.4) and applied at 20-22 ºC for 2h. EdU (28) was visualized with Alexa 647-azide using Click-iT labeling (Life Technologies). Salispheres were counterstained with

Hoechst 33,342 (Sigma) and then coverslipped with Fluoromount (Sigma). Orthogonal stacks of salispheres were imaged using a Zeiss LSM-880 confocal microscope. $DAPI^+$ and EdU^+ cells were counted automatically with Imaris.

Mouse salisphere cultures

Adult male *Tau2*-EGFP mice (n = 2/experiment) (29) were used for all in vitro experiments described since we find EGFP expression selectively in granulated ducts (Supporting Fig. 2H). Mice older than 3 months were used as cultures from younger mice did not respond consistently to acetylcholine (5 µM, Tocris) in our Ca^{2+}-imaging protocols. We have modified previously published salisphere protocols to make them compatible with our experimental aims (30). In brief, submandibular glands were dissected and mechanically dissociated (by trituration using 100 µl pipette tips). Subsequently, cells were enzymatically dissociated in two cycles with hyaluronidase (Sigma) and subsequently collagenase II (Sigma) under continuous agitation at 37 ˚C for 40 min per each step. Cell clusters were centrifuged (400 *g*), washed twice and filtered with a mesh of 100-µm pore size to remove debris and undigested cell aggregates. Next, cell clusters were sequentially filtered through meshes of 40- and 20 µm pore size. The 20-µm mesh was flipped and clusters washed off to only collect cell clusters between 20 and 40-µm in diameter, thus ensuring approximately equal cell cluster size at the start of the proliferation assays. Cell clusters were plated in F12 medium (Invitrogen) containing penicillin (100 U/mL; Gibco), streptomycin (100 µg/mL; Gibco), Glutamax (2 mM; Gibco), epidermal growth factor-2 (20 ng/mL; Invitrogen), basic fibroblast growth factor (20 ng/mL; Invitrogen), N2 supplement (1%; Invitrogen), insulin (10 µg/mL; Sigma) and dexamethasone (1 µM; Invitrogen) overnight. The following day, clusters were collected by centrifugation and re-suspended in culture medium for plating on top of a layer of Matrigel matrix (1:1; Corning) molten on glass coverslips (in 24-well plates) for cell proliferation experiments and Ca^{2+} imaging. For experiments with cellular maturation, we used smaller clusters (starting with 3-5 cells / cluster) to limit differentiated cell content. Small stem cell clusters were directly plated in medium containing LPI or CID 16020046 and fixed on day 1, 3 and 5 after plating. Note that survival of smaller clusters was compromised (except when treated with CID 16020046) as compared to 20 and 40-µm clusters, as shown by the decrease in cluster size after prolonged culturing in vitro.

Experiments on salispheres from *Gpr55*$^{-/-}$ mice proved difficult as the Matrigel under the cells was digested away by 1 day after plating (Supporting Fig. 5I,J). This matrix loss could be prevented by addition of 10% fetal bovine serum (FBS), however, inadvertently making these experiments uncomparable to previous serum-free experiments (especially in light of cell proliferation).

Ca^{2+} imaging

Salispheres, isolated from Tau2-EGFP mice, were loaded with Ca^{2+} dye Fura-2AM (Invitrogen) for 30 min at 37˚C. Ratiometric $[Ca^{2+}]_I$ measurements were performed at 20-24 ºC temperature selectively on $EGFP^+$ clusters with continuous superfusion with oxygenated Krebs-Ringer solution (in mM: 119 NaCl, 2.5 KCl, 1 NaH_2PO_4, 1.5 $CaCl_2$ and 1.5 $MgCl_2$, 20 HEPES, 3 glucose, pH7.4). Drugs where applied in bath at the following concentrations: 5 µM ACh (Sigma), 3 µM LPI (Sigma), 1 µM N-PCC, 3 µM CID 16020046 (Tocris). We observed occasional baseline elevation, most likely due to the embedding of salispheres in matrigel, leading to accumulation of ACh in the gel. We used a VisiChrome monochromator (Visitron Systems, 340/380 nm excitation) and a CoolSnap HQ^2 back-cooled camera (Photometrics) mounted onto a Zeiss Axiovert microscope equipped with a water-immersion 40×/differential interference contrast objective (Plan-Apochromat/N.A. 1.0) to perform Fura-2AM/Ca^{2+} imaging. VisiView software (Visitron Systems) was used to measure Fura-2AM fluorescence, which was expressed as a change in the ratio of ΔF340/F380 fluorescence that is proportional to the concentration of cytosolic Ca^{2+}.

Image analysis

Single images containing salivary glands were exported from digitalized slides using NDP.view (NanoZoomer Digital Pathology Image) and densitometrically analysed. Images were cropped out using a free-hand tool at 10x magnification. Quantitative analysis of immunoreactivity was performed in ImageJ (NIH, 1.50g): after color deconvolution to spectrally unmix the hematoxylin pigment (Color Deconvolution Plugin), images were converted to 8-bit resolution. The threshold defining immunopositivity was set case-by-case to equalize background stainings. Area coverage (%) of immunopositive structures was calculated for all exported images and expressed as percentage of the total surface area. For carcinomas, images from non-transformed tissues adjacent to histopathologically-defined tumour cells (5 areas per section) were compared to tumour tissues within the same section. Irradiated cases (containing no healthy tissue) were compared to other healthy control cases (Supporting Table 1). Thus, we aimed to minimize potential technical bias that had been due to different fixation and variability of enzymatic (DAB) reactions. In parallel, a semi-quantitative approach was adopted to score individual structures of each gland (striated duct, intercalated duct, serous acini and mucous acini) for GPR55 immunoreactivity on a scale of 0 to 3 (3 being the strongest staining). Carcinoma tissues on the same section were scored similarly and plotted against all healthy structures.

Legends to SI Figures and Tables

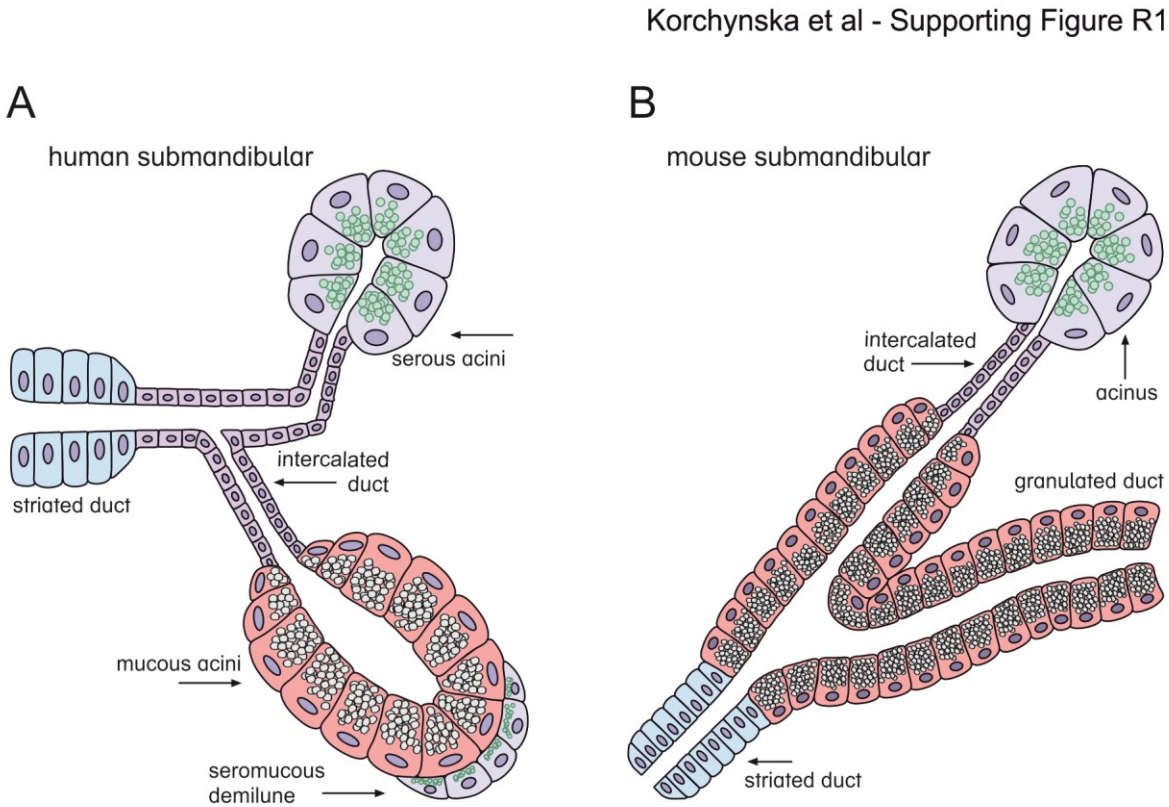

Supporting Fig. 1 *Submandibular gland morphology*. (**A,B**) Schematic overview of gross morphological differences between mouse and human submandibular glands. Note the lack of mucous acini in the mouse gland.

Korchynska et al - Supporting Figure R2

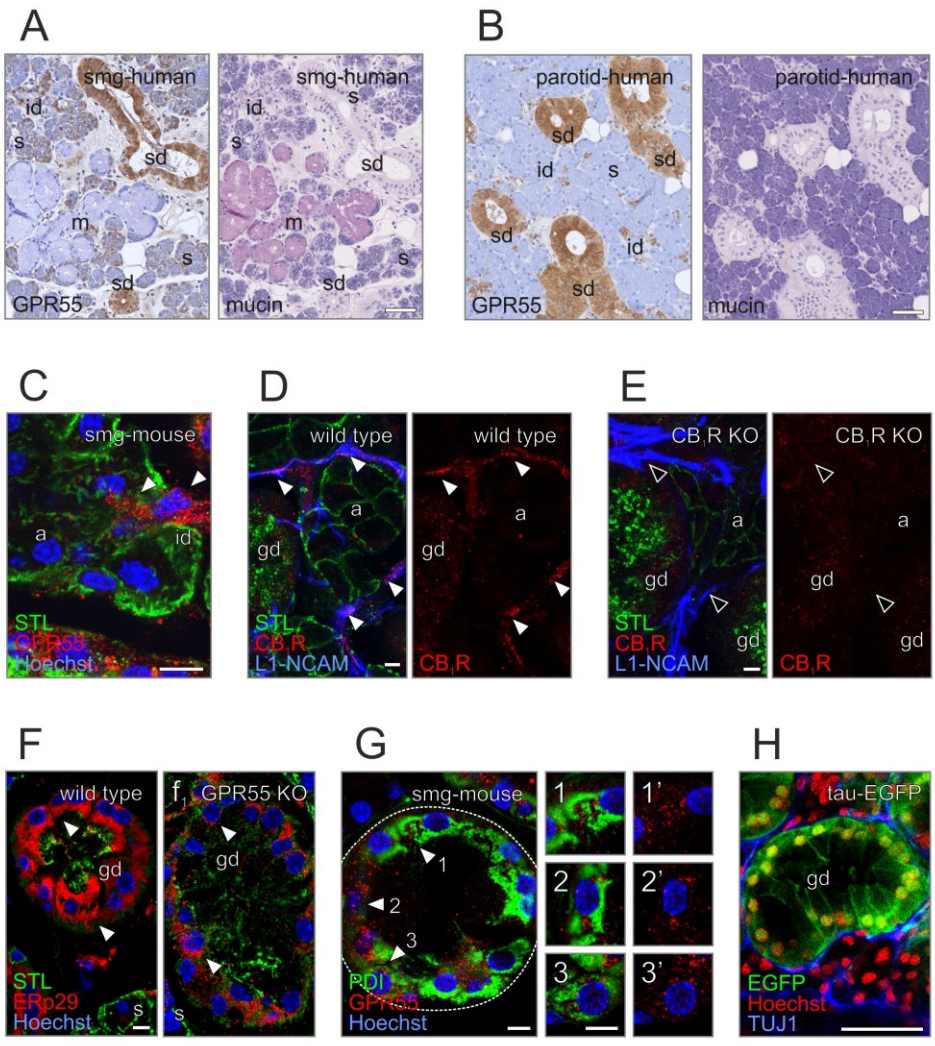

Supporting Fig. 2 *GPR55 localization in major salivary glands*. (**A,B**) Cellular distribution pattern of GPR55 in *human* submandibular (A) and parotid glands (B). Mucin staining was performed to identify mucous acinar. (**C**) GPR55 immunoreactivity was not observed in *mouse* acini. Arrowheads indicate unspecific binding in intercalated ducts. (**D,E**) CB_1R staining in submandibular glands is limited to L1-$NCAM^+$ nerve bundles (arrowheads). Note the lack of staining in the *Cnr1*$^{-/-}$ gland. (**F**) Endoplasmic reticulum staining in wild type *vs*. *Gpr55*$^{-/-}$ mouse granulated ducts. Arrowheads indicate diminished ERp29 immunoreactivity. (**G**) PDI labelling shows the presence of GPR55 close to the endoplasmic reticulum. (**H**) *Tau2*-EGFP transgenic mice harbour EGFP specifically in granulated ducts of the submandibular gland. Abbreviations: a, acini; gd, granulated duct; id, intercalated duct; m, mucous acini; s, serous acini; sd striated duct. *Scale bars* = 50 µm (A,B), 25 µm (H), 10 µm (C,D,E,F,G).

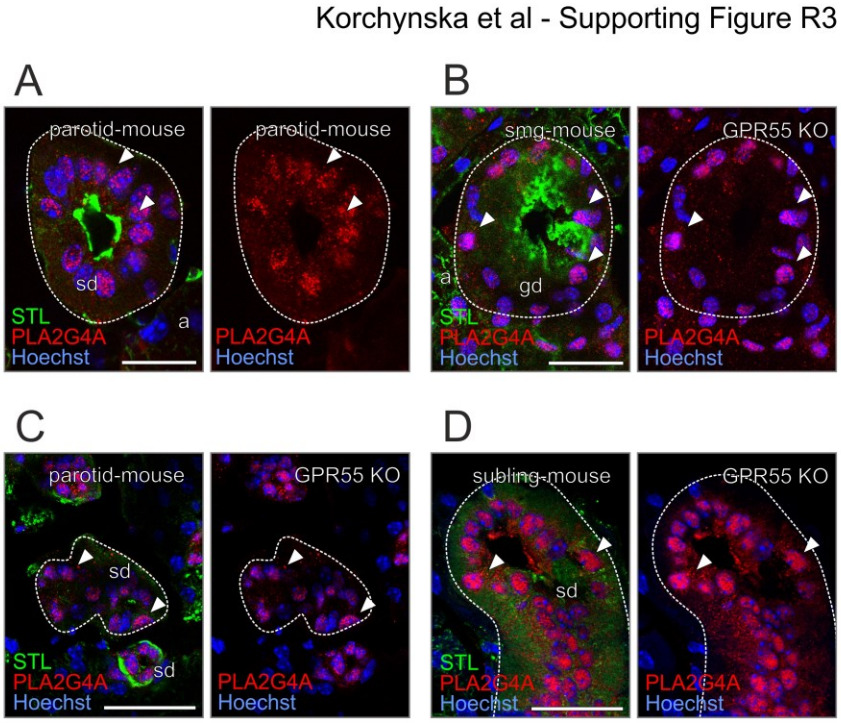

Supporting Fig. 3 *PLA2G4A localization in ductal structures*. (**A-D**) PLA2G4A immunoreactivity (*arrowheads*) in mouse wild type and *Gpr55*$^{-/-}$ parotid (A,C), submandibular (B) and sublingual (D) glands. PLA2G4A staining in striated ducts revealed no difference as compared to wild type controls. Abbreviations: gd, granulated duct; sd striated duct. *Scale bars* = 30 µm (A,B,C,D).

Korchynska et al - Supporting Figure R4

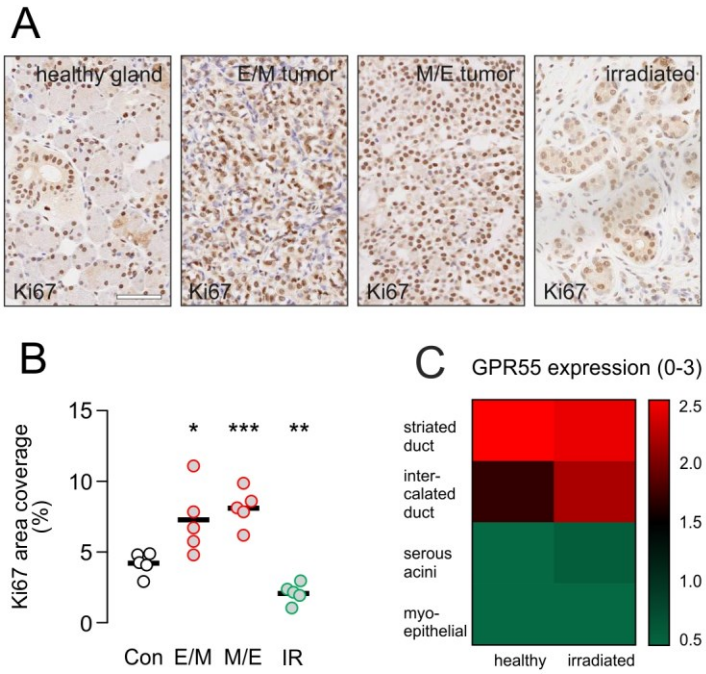

Supporting Fig. 4 *Proliferation rates in carcinomas and after irradiation therapy*. (**A,B**) Ki67 labeling was significantly increased in epithelial-myoepithelial (E/M) and mucoepidermoid carcinomas (M/E), as compared to healthy controls (con). Irradiation therapy largely inhibited proliferation (B). (C) Heat maps showing GPR55 expression in various cellular compartments of irradiated cases. *Scale bar* = 100 µm (A). **P* < 0.05, ***P* < 0.01, ****P* < 0.001.

Korchynska et al - Supporting Figure R5

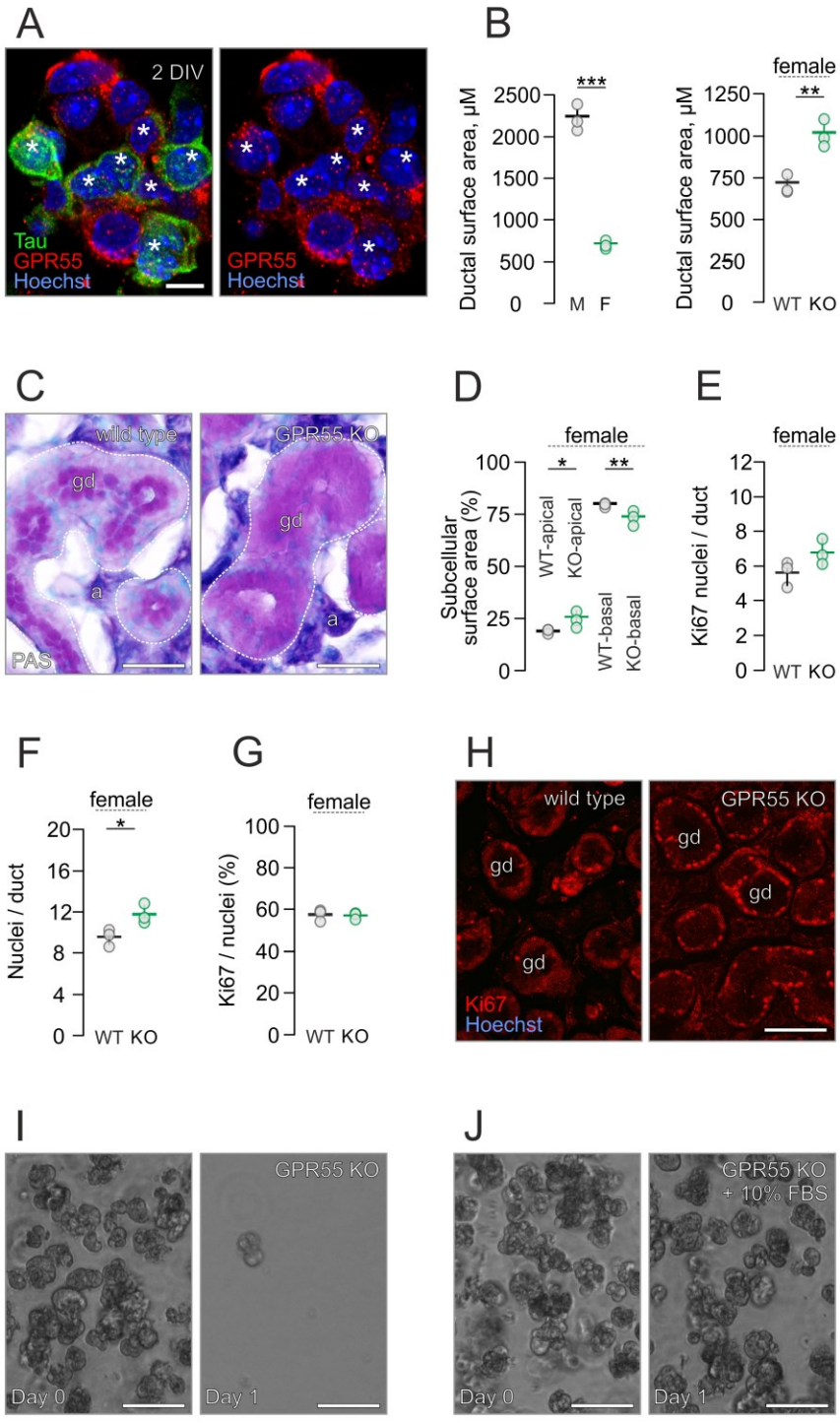

Supporting Fig. 5 *GPR55 deletion increases cell proliferation in submandibular ducts*. (**A**) After two days in vitro, GPR55 is expressed by most cells in cultured salispheres. (**B**) Ductal surface area measured between males and females, as well as female wild type *vs. Gpr55*$^{-/-}$ submandibular glands. (**C**) Glycoprotein staining with periodic acid Schiff (*purple*) in granular ducts of both wild type and *Gpr55*$^{-/-}$ submandibular gland. (**D**) Basal *vs*. apical surface measurements in wild type and *Gpr55*$^{-/-}$ female mice. (**E-H**) Ki67 immunoreactivity in female *Gpr55*$^{-/-}$ submandibular granulated ducts. (**I,J**) *Gpr55* salispheres digested their basement membrane matrix the day after plating. Addition of 10% FBS prevented this extracellular enzyme activity (J). Abbreviations: a, acini; gd, granulated duct. *Scale bars* = 50 µm (C), 25 µm (I,J), 10 µm (A). *$P < 0.05$

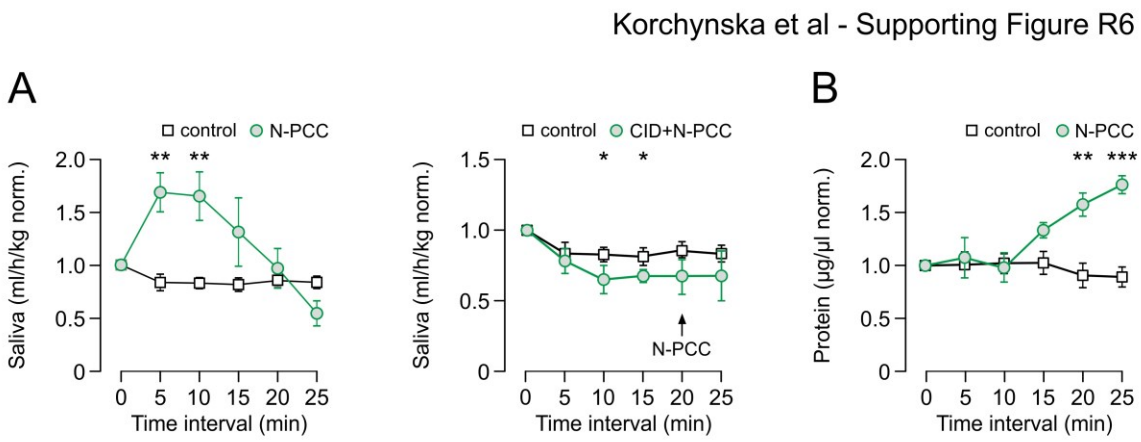

Supporting Fig. 6 *GPR55 controls salivation in the rat*. (**A**) N-PCC injections into the rat submandibular gland significantly induce salivation. Pretreatment with CID occluded this response. (B) Salivary protein content significantly increased after N-PCC treatment. **P* < 0.05, ***P* < 0.01, ****P* < 0.001

Supporting Table 1 – List of cases used in this study. Tissues were obtained and used in accordance with the Declaration of Helsinki and compatible institutional guidelines (Medical University of Vienna).

Case#	Gender	D.O.B.	Condition
6170	M	03-08-1951	Control
9272	F	21-12-1939	Control
21505	F	28-10-1957	Control
24528	F	13-12-1948	Control
25678	M	04-05-1939	Control
1038	M	09-07-1940	Irradiated
13517	M	16-12-1946	Irradiated
15094	M	09-02-1967	Irradiated
18077	M	12-08-1927	Irradiated
19956	M	17-02-1927	Irradiated
23919	F	04-05-1944	Irradiated
4053	M	06-04-1947	Epithelial-myoepithelial carcinoma
6765	M	25-03-1924	Epithelial-myoepithelial carcinoma
11567	F	05-02-1922	Epithelial-myoepithelial carcinoma
12893	F	29-10-1919	Epithelial-myoepithelial carcinoma
13352	M	25-09-1938	Epithelial-myoepithelial carcinoma
22177	F	06-05-1954	Epithelial-myoepithelial carcinoma
1561	M	29-01-1962	Mucoepidermoid carcinoma
6257	F	21-04-1955	Mucoepidermoid carcinoma
10780	F	05-08-1963	Mucoepidermoid carcinoma
10817	F	19-02-1980	Mucoepidermoid carcinoma
13361	F	20.01.1943	Mucoepidermoid carcinoma
20347	F	05-05-1984	Mucoepidermoid carcinoma
23653	M	11-03-1926	Mucoepidermoid carcinoma
23684	F	14-10-1959	Mucoepidermoid carcinoma

Supporting Table 2 – List of qPCR primer pairs used in this study.

Probe name	Sequence (5'-3')	Size (bp)
Cnr1 Mouse Forward	TCT TAG ACG GCC TTG CAG AT	162
Cnr1 Mouse Reverse	AGG GAC TAC CCC TGA AGG AA	
Cnr2 Mouse Forward	TCA GAC TGG GCC CAG TCT T	199
Cnr2 Mouse Reverse	GCG CTC AGC AGC CCC ATC AG	
Gpr55 Mouse Forward 1	GTC CAT ATC CCC ACC TTC CT	168
Gpr55 Mouse Reverse 1	CAT CTT GAA TGG GAG GGA GA	
Gpr55 Mouse Forward 2	TCA CCA TCT GCT TCA TCA GC	161
Gpr55 Mouse Reverse 2	CAC TTC CCT GTG GAA GGT GT	

Supporting Table 3 – List of markers used in this study. Abbreviations: Gt, goat; Ms, mouse; Rb, rabbit. Mouse GPR55 epitope: KEFRMRIKAHRPSTIKLVNQDTMVSRG

Marker	Mouse	Human	Host	Source
CB_1R	1:1000	-	Gt	Dr. Watanabe
Cleaved caspase-3	1:500		Rb	Cell Signaling Tech Cat. No. 9661
ERp29	1:500	1:250	Rb	Thermofisher Cat. No. PA3-011
GFP	1:1,000	-	Gt	Abcam Cat. No. ab6662
GPR55	1:4,000 - 16,000	1:100	Rb	Dr. Mackie
Hoechst 33,342	1:10,000	-	-	Sigma Cat. No. B2261
Ki67	1:100	1:100	Rb	Millipore Cat. No. AB9260
L1-NCAM	1:1000	-	Rt	Millipore Cat. No. MAB5272
PDI	1:200	1:100	Ms	Millipore, out of production
PH3	1:200	-	Rb	Cell Signaling Tech Cat. No. 9701S
PLA2G4A	1:1000	1:50	Rb	Atlas Antibodies Cat. No. HPA050062
Solanum tuberosum lectin	1:100	-	-	Vector Cat. No. B1165
Sox2	1:1000		Rb	Abcam Cat. No. ab97959
Sox10	1:500		Gt	R&D Systems Cat. No. AF2864
TUJ1	1:2,000	-	Ms	Promega Cat. No. G7121

Supporting References

1. Stella N, Schweitzer P, Piomelli D. A second endogenous cannabinoid that modulates long-term potentiation. *Nature* 1997;388(6644):773–778.

2. Devane WA et al. Isolation and structure of a brain constituent that binds to the cannabinoid receptor. *Science* 1992;258(5090):1946–1949.

3. Matsuda LA, Lolait SJ, Brownstein MJ, Young AC, Bonner TI. Structure of a cannabinoid receptor and functional expression of the cloned cDNA. *Nature* 1990;346(6284):561–564.

4. Munro S, Thomas KL, Abu-Shaar M. Molecular characterization of a peripheral receptor for cannabinoids. *Nature* 1993;365(6441):61–65.

5. Ryberg E et al. The orphan receptor GPR55 is a novel cannabinoid receptor. *Br. J. Pharmacol.* 2007;152(7):1092–1101.

6. Kopach O et al. Cannabinoid receptors in submandibular acinar cells: functional coupling between saliva fluid and electrolytes secretion and Ca2+ signalling. *J. Cell Sci.* 2012;125(Pt 8):1884–1895.

7. Prestifilippo JP et al. Inhibition of salivary secretion by activation of cannabinoid receptors. *Exp. Biol. Med. Maywood NJ* 2006;231(8):1421–1429.

8. Graham ES, Angel CE, Schwarcz LE, Dunbar PR, Glass M. Detailed characterisation of CB2 receptor protein expression in peripheral blood immune cells from healthy human volunteers using flow cytometry. *Int. J. Immunopathol. Pharmacol.* 2010;23(1):25–34.

9. Jiang W et al. Cannabinoids promote embryonic and adult hippocampus neurogenesis and produce anxiolytic- and antidepressant-like effects. *J. Clin. Invest.* 2005;115(11):3104–3116.

10. Prenderville JA, Kelly ÁM, Downer EJ. The role of cannabinoids in adult neurogenesis. *Br. J. Pharmacol.* 2015;172(16):3950–3963.

11. Kano M, Ohno-Shosaku T, Hashimotodani Y, Uchigashima M, Watanabe M. Endocannabinoid-mediated control of synaptic transmission. *Physiol. Rev.* 2009;89(1):309–380.

12. Liu LY et al. Cannabinoid receptor signaling regulates liver development and metabolism. *Dev. Camb. Engl.* 2016;143(4):609–622.

13. Chiurchiù V, Battistini L, Maccarrone M. Endocannabinoid signalling in innate and adaptive immunity. *Immunology* 2015;144(3):352–364.

14. Miller AM, Stella N. CB2 receptor-mediated migration of immune cells: it can go either way. *Br. J. Pharmacol.* 2008;153(2):299–308.

15. Turcotte C, Blanchet M-R, Laviolette M, Flamand N. The CB2 receptor and its role as a regulator of inflammation. *Cell. Mol. Life Sci.* 2016;73(23):4449–4470.

16. Jin Y et al. Sphingosine 1-phosphate is a novel inhibitor of T-cell proliferation. *Blood* 2003;101(12):4909–4915.

17. Liu G, Yang K, Burns S, Shrestha S, Chi H. The S1P(1)-mTOR axis directs the reciprocal differentiation of T(H)1 and T(reg) cells. *Nat. Immunol.* 2010;11(11):1047–1056.

18. Garris CS et al. Defective sphingosine 1-phosphate receptor 1 (S1P1) phosphorylation exacerbates TH17-mediated autoimmune neuroinflammation. *Nat. Immunol.* 2013;14(11):1166–1172.

19. Gao J et al. Stimulating Beta Cell Replication and Improving Islet Graft Function by a GPR40 and GPR120 Dual Agonist: 2573. *Transplantation* 2012;94(10S):567.

20. Ansarullah et al. Stimulating β-Cell Regeneration by Combining a GPR119 Agonist with a DPP-IV Inhibitor [Internet]. *PLoS ONE* 2013;8(1). doi:10.1371/journal.pone.0053345

21. Huan Y et al. The dual DPP4 inhibitor and GPR119 agonist HBK001 regulates glycemic control and beta cell function ex and in vivo. *Sci. Rep.* 2017;7(1):4351.

22. Edfalk S, Steneberg P, Edlund H. Gpr40 is expressed in enteroendocrine cells and mediates free fatty acid stimulation of incretin secretion. *Diabetes* 2008;57(9):2280–2287.

23. Zhang D et al. Insulinotropic effects of GPR120 agonists are altered in obese diabetic and obese non-diabetic states.. *Clin. Sci. Lond. Engl. 1979* 2017;131(3):247–260.

24. Hurst K et al. A putative lysophosphatidylinositol receptor GPR55 modulates hippocampal synaptic plasticity. *Hippocampus* 2017;27(9):985–998.

25. Sylantyev S, Jensen TP, Ross RA, Rusakov DA. Cannabinoid- and lysophosphatidylinositol-sensitive receptor GPR55 boosts neurotransmitter release at central synapses. *Proc. Natl. Acad. Sci. U. S. A.* 2013;110(13):5193–5198.

26. Cembrowski MS, Wang L, Sugino K, Shields BC, Spruston N. Hipposeq: a comprehensive RNA-seq database of gene expression in hippocampal principal neurons. *eLife* 2016;5:e14997.

27. Paulsen FP et al. Similarities and differences in lectin cytochemistry of laryngeal and tracheal epithelium and subepithelial seromucous glands in cases of sudden infant death and controls. *Thorax* 2001;56(3):223–227.

28. Zeng C et al. Evaluation of 5-ethynyl-2'-deoxyuridine staining as a sensitive and reliable method for studying cell proliferation in the adult nervous system. *Brain Res.* 2010;1319:21–32.

29. Tucker KL, Meyer M, Barde YA. Neurotrophins are required for nerve growth during development. *Nat. Neurosci.* 2001;4(1):29–37.

30. Pringle S, Nanduri LSY, Marianne van der Z, Ronald van O, Coppes RP. Isolation of Mouse Salivary Gland Stem Cells. *JoVE J. Vis. Exp.* 2011;(48):e2484–e2484.